



**HAL**  
open science

# Tuning the Aggregation Behaviour of BN-Coronene Diimides with the Imide Substituents and their Performance in Devices (OLED, OFET)

Jonas Hoffmann, Bernard Geffroy, Emmanuel Jaques, Muriel Hissler, Anne Staubitz

► **To cite this version:**

Jonas Hoffmann, Bernard Geffroy, Emmanuel Jaques, Muriel Hissler, Anne Staubitz. Tuning the Aggregation Behaviour of BN-Coronene Diimides with the Imide Substituents and their Performance in Devices (OLED, OFET). *Journal of Materials Chemistry C*, 2021, 9 (41), pp.14720-14729. 10.1039/D1TC02991F . hal-03372700

**HAL Id: hal-03372700**

**<https://hal.science/hal-03372700>**

Submitted on 11 Oct 2021

**HAL** is a multi-disciplinary open access archive for the deposit and dissemination of scientific research documents, whether they are published or not. The documents may come from teaching and research institutions in France or abroad, or from public or private research centers.

L'archive ouverte pluridisciplinaire **HAL**, est destinée au dépôt et à la diffusion de documents scientifiques de niveau recherche, publiés ou non, émanant des établissements d'enseignement et de recherche français ou étrangers, des laboratoires publics ou privés.

# Tuning the Aggregation Behaviour of BN-Coronene Diimides with the Imide Substituents and their Performance in Devices (OLED, OFET)

Jonas Hoffmann,<sup>a,b,c</sup> Bernard Geffroy,<sup>d</sup> Emmanuel Jaques,<sup>e</sup> Muriel Hissler\*<sup>c</sup> and Anne Staubitz\*<sup>a,b</sup>

Compared to perylene diimides (**PDI**s), the coronene diimides (**CDI**s), which can be viewed as a lateral core extension, show undesired effects for optoelectronic devices such as the decrease of the absorption and a hypsochromic shift. Here, we demonstrate that if the core is extended with two BN units as opposed to two CC units, the opposite is true: Large bathochromic shifts can be achieved, together with higher molar extinction coefficients and beneficial luminescence properties, e.g. a small Stokes shift and high quantum yields ( $\Phi_{\text{lum}} > 94\%$ ). These effects can be explained by the influence of the BN-unit onto the frontier molecular orbitals of the **BNCDI**. Different substitution motifs at the imide-position, cyclohexyl and 2,6-diisopropylphenyl, although they had no influence on the optical properties on a single molecule level, influenced the aggregation substantially so that the optical properties in the solid-state and the performance in organic devices (OLED and OFET) differed considerably. In combination with host matrices devices with EQE up to 1.5% and white light emission (0.317; 0.346) were obtained. The developed synthetic route starting from a regioisomeric pure 1,7-substituted PDI leads to **BNCDI**s in good yields, which makes this class of compounds very promising.

## Introduction

Polycyclic aromatic hydrocarbons (PAHs) have a leading role as active components in organic electronics due to their excellent electronic and optoelectronic properties.<sup>1-5</sup> The molecular engineering of PAHs allows tuning the gap between the highest occupied molecular orbital (HOMO) and the lowest unoccupied molecular orbital (LUMO) respectively.<sup>6</sup> This promoted the application of PAHs in organic electronics such as in organic solar cells (OSC), organic field-effect transistors (OFET), and organic light-emitting devices (OLED).<sup>7-11</sup> However, the variety of PAH-based  $\pi$ -conjugated non-fullerene electron acceptors remains limited. The most popular class of these compounds are rylene diimides, which are polycyclic aromatic chromophores based on two, side-on fused naphthalene units that are capped with two imide groups. These PAHs are widely used in the dye industry,<sup>12</sup> fluorescence labelling,<sup>13, 14</sup> and foremost in organic semiconducting devices.<sup>15</sup> In particular, perylene diimides (**PDI**s) and naphthalene diimides (**NDI**s) are

the most prominent rylene diimides because of their outstanding photochemical and thermal stability.<sup>16</sup> Extending rylene diimides in their long molecular axis narrows the HOMO-LUMO gap, while the extension of the short molecular axis widens the HOMO-LUMO gap.<sup>17, 18</sup> In the case of **PDI** and coronene diimide (**CDI**), this leads to a blueshift of the absorption maximum from 525 nm (in **PDI**s) to 494 nm (in **CDI**s), a threefold decrease of the extinction coefficient, and a hypsochromic effect on the maximum of emission (532 nm to 500 nm) (Fig. 1). Moreover, a reduction of the fluorescence quantum yield ( $\Phi_{\text{lum}} = 0.98$  to 0.69) occurs, which is detrimental for many devices.<sup>19</sup> The main reason for such photophysical changes can be found in the organization of the frontier orbitals. While the bay-extension from **PDI** to **CDI** leaves the LUMO unchanged, it influences the orientation of the HOMO level: In **PDI**s the HOMO level is located along the molecular axis, but in **CDI**s it is oriented along the short molecular axis leading to a reduced orbital coefficient in the HOMO-LUMO.<sup>20, 21</sup> An alternative to the extension of the  $\pi$ -system of the carbon scaffold is the integration of heteroatoms (B, N, Si, P) which effectively modifies the HOMO-LUMO gap.<sup>22</sup> In addition, the combination of two heteroelements represents a versatile tool to influence the frontier orbitals of a PAH, but is less likely to distort the flat geometry of the molecule. In particular, the isoelectronic substitution of a C=C unit with a B=N unit (BN/CC isosterism) became a prominent design principle in recent years.<sup>23-27</sup> This isoelectronic substitution can alter the frontier-orbital energies, stabilize the HOMO,<sup>28-32</sup> and significantly alter the orbital distribution of the resulting BN-PAH compared to the corresponding carbonaceous congeners.<sup>33, 34</sup> In fact, it was found that as a general rule, BN-substitution provides a

<sup>a</sup> University of Bremen, Institute for Organic and Analytical Chemistry, Leobener Straße 7, D-28359 Bremen, Germany. Email: [staubitz@uni-bremen.de](mailto:staubitz@uni-bremen.de).

<sup>b</sup> University of Bremen, MAPEX Center for Materials and Processes, Bibliothekstraße 1, D-28359 Bremen, Germany.

<sup>c</sup> ISCR, Institut des Sciences Chimiques de Rennes, UMR 6226, CNRS-Université de Rennes 1, Campus de Beaulieu, 35042 Rennes Cedex, France. Email: [muriel.hissler@univ-rennes1.fr](mailto:muriel.hissler@univ-rennes1.fr).

<sup>d</sup> Université Paris-Saclay, CEA, CNRS, NIMBE, LICSEN, 91191, Gif-sur-Yvette, France.

<sup>e</sup> IETR, Institut d'Électronique et de Télécommunications de Rennes, UMR 6164, CNRS-Université de Rennes 1, Campus de Beaulieu, 35042 Rennes Cedex, France.

† Footnotes relating to the title and/or authors should appear here.

Electronic Supplementary Information (ESI) available: Experimental conditions, full characterizations, <sup>1</sup>H NMR, <sup>11</sup>B NMR and <sup>13</sup>C NMR spectra of all new compounds, UV-Vis, fluorescence and OFET/OLED production as well as computational details.

bathochromic shifted absorption, higher fluorescence quantum yield and high hole mobility maintaining high thermal and photochemical stability.<sup>29, 30, 35-40</sup>

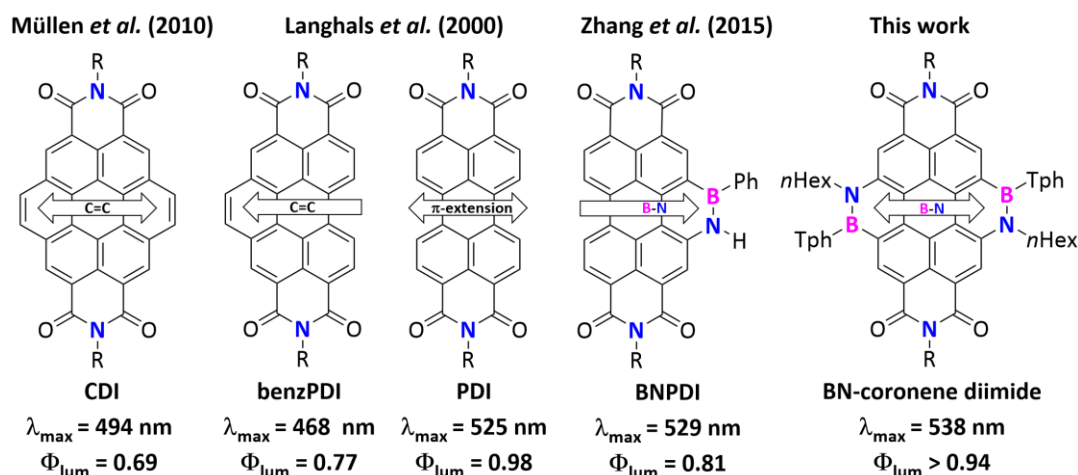


**Fig. 1** The bay extension from perylene diimide (PDI)<sup>41</sup> via benzannulated perylene diimide (benzPDI)<sup>19</sup> to coronene diimide (CDI)<sup>42</sup> led to a hypsochromic shift of the absorption. Contrarily, the bay extension from perylene diimide (PDI), via BNPDI to the BN-coronene diimide (BNCDI) (this work) resulted in a red-shifted absorption.

In fact, a boron/nitrogen-*mono*-substituted PDI (BNPDI) has already been reported, which had a substantial bathochromic shift (61 nm) compared to the respective all-carbon benzPDI.<sup>19, 43</sup> The integration of the cyclohexyl-substituted BNPDI<sup>Cy</sup> in OLED devices, revealed aggregation-caused quenching (ACQ) effects which reduced the overall performance in OLED devices. Such an aggregation phenomenon is well investigated in PAHs,<sup>44</sup> especially rylene diimides, as they have a strong tendency to undergo intermolecular  $\pi$ - $\pi$  stacking.<sup>45</sup> While these aggregates are desirable for charge transport,<sup>46, 47</sup> they result in adverse photophysical properties of the rylene diimides when aggregated, e.g. ACQ, and further hamper their device processing. To prevent aggregation of rylene diimides, the functionalization of the *bay*-area,<sup>45, 48, 49</sup> the *ortho*-positions,<sup>50, 51</sup> or the imide positions<sup>41, 52, 53</sup> became common. The latter method has the advantage that it leaves the rylene core unaffected as the imide substituent is electronically decoupled from the rylene core.<sup>54</sup>

The effect of a BN-substitution of coronene diimide (CDI) to give the BN-analog BNCDI and the resulting optoelectronic properties were studied. This should provide a deeper insight into how BN-substitution alters the HOMO/LUMO levels of PAHs. Furthermore, two different imide substituents and their

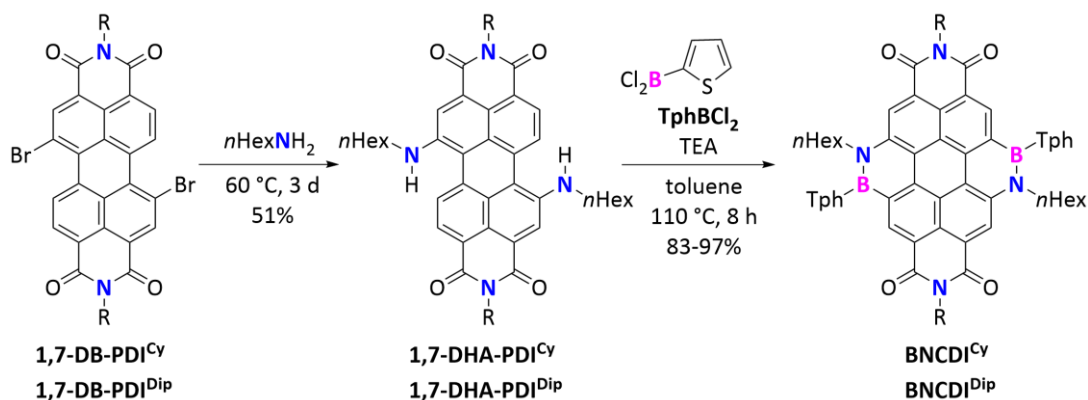
effect on the solid-state properties of the BNCDIs was investigated.

As examples, the structures of the thienyl-substituted BNCDIs with prominent cyclohexyl (Cy) or diisopropylphenyl (Dip) substituents<sup>19</sup> at the imide's nitrogen were chosen (Fig. 2).

## Results and Discussion

### Synthesis of the BNCDIs

Starting from the regioisomerically pure 1,7-brominated PDIs (**1,7-DB-PDI<sup>Cy/Dip</sup>**), generated *via* bromination of perylene tetraesters,<sup>55</sup> we implemented the *n*hexylamino moiety by an aromatic nucleophilic substitution (Scheme 1). Although several protocols for the reaction of neat primary alkylamines and 1,7-brominated PDIs at high temperatures were published,<sup>56-58</sup> the yields and high formation of side products (monosubstitution and dehalogenation forming the 1-alkylamino-PDI) were unsatisfactory. To prevent the dehalogenation of the intermediary 1-alkyl-7-bromo-PDI (**1,7-DB-PDI<sup>Cy/Dip</sup>**), we lowered the reaction temperature to 60 °C with a concomitant extension of the reaction time to 3 d. Using this protocol, we



---

**Scheme 1** Synthesis of BN-substituted **BNCDIs** through amination of **1,7-DB-PDI** and ring annulation reaction of **1,7-DHA-PDI** with **TphBCl<sub>2</sub>**. Tph: Thiophenyl. Details can be found in the ESI.

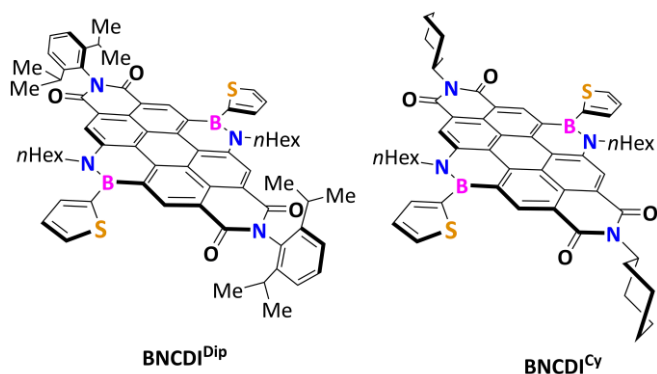
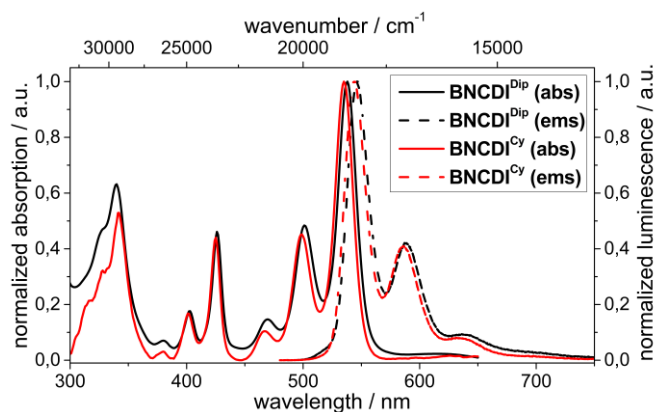


**Fig. 2** Molecular structures of **BNCDI<sup>Cy</sup>** and **BNCDI<sup>Dip</sup>** which only differ in their imide functionality.

could obtain both 1,7-di(*n*hexylamino)-PDIs (**1,7-DHA-PDI<sup>Cy/Dip</sup>**) in a moderate yield of 51% after intense column chromatography. In a final step, the **BNCDIs** were formed by the reaction of **1,7-DHA-PDI<sup>Cy/Dip</sup>** with 2-thienyldichloroborane (**TphBCl<sub>2</sub>**) and triethylamine as a base in high yields (97%/83%). The resulting purple/red amorphous powders showed good solubility in halogenated solvents, toluene, and THF. Furthermore, **BNCDIs** showed stability against moisture, strongly acidic and basic conditions. We fully characterized the **BNCDIs** by <sup>1</sup>H/<sup>11</sup>B/<sup>13</sup>C NMR-, and FTIR spectroscopies and high-resolution mass spectrometry. Since the aromatic perylene protons gave rise to only two proton signals and the carbon atoms located at the imide position gave rise to also only two signals, both **BNCDIs** were of C<sub>2</sub>-symmetry and were therefore regioisomerically pure (see also the ESI for detailed experimental conditions and full characterization of all compounds). Attempts to grow crystals failed throughout using different techniques as only aggregates were observed.

#### Optical properties of the **BNCDIs** in solution

To evaluate the effect of the BN-substitution on the **CDI** scaffold, the optical properties of the **BNCDIs** were analyzed by UV/Vis absorption and fluorescence spectroscopy in DCM. The absorption spectra of both **BNCDIs** were characterized by their intense maxima at 535/538 nm (**BNCDI<sup>Cy</sup>/BNCDI<sup>Dip</sup>**) and high extinction coefficients ( $\epsilon \approx 70794\text{--}74131 \text{ M}^{-1} \text{ cm}^{-1}$ ) (Fig. 3, Table 1). The absorption bands exhibited well-resolved typical vibronic fine structures with the strongest transition ( $S_0 \rightarrow S_1$ ) at 535/538 nm with further transitions at 498/501 nm and 466/470 nm from the 0-0, 0-1 and 0-2 vibronic bands. The higher energetic transitions ( $S_0 \rightarrow S_2$ ) occurred at 425/426 nm and 401/401 nm for the respective 0-0 and 0-1 vibronic transitions.<sup>59, 60</sup> Moreover, a distinct absorption band is found between 300-350 nm. As expected, the effect of the imide sub-



<sup>a</sup> Measured in DCM ( $1.0 \times 10^{-6} \text{ M}$ ). <sup>b</sup> Obtained from the offset wavelength derived from the low energy absorption band. <sup>c</sup> Referenced against fluorescein in 0.1 M NaOH.

**Fig. 3** Absorption and emission spectra of compounds **BNCDI<sup>Cy</sup>** and **BNCDI<sup>Dip</sup>**. Photographic images of both **BNCDIs** at ambient light (left) and with irradiation of light (365 nm) exhibiting green luminescence (right).

stituents (**Cy** or **Dip**) the optical properties was marginal in solution.<sup>41</sup>

Both **BNCDI<sup>Cy</sup>** and **BNCDI<sup>Dip</sup>** exhibited a strong luminescence ( $\Phi_{\text{lum}}(\text{BNCDI}^{\text{Cy}}/\text{BNCDI}^{\text{Dip}}) = 0.94/0.95$ ) and small Stokes shifts ( $\Delta\nu_{\text{Stokes}}(\text{BNCDI}^{\text{Cy}}/\text{BNCDI}^{\text{Dip}}) = 310/272 \text{ cm}^{-1}$ ) in DCM solution indicating a high rigidity of the molecule in the ground state and the excited state. As expected for such a system, the bands were mirror images of the absorbance spectra including the vibronic fine structure with bands at 545/546 nm, 585/588 nm and 634/638 nm. This was attributed to the  $S_1 \rightarrow S_0$  transitions and the respective vibronic bands.<sup>61</sup>

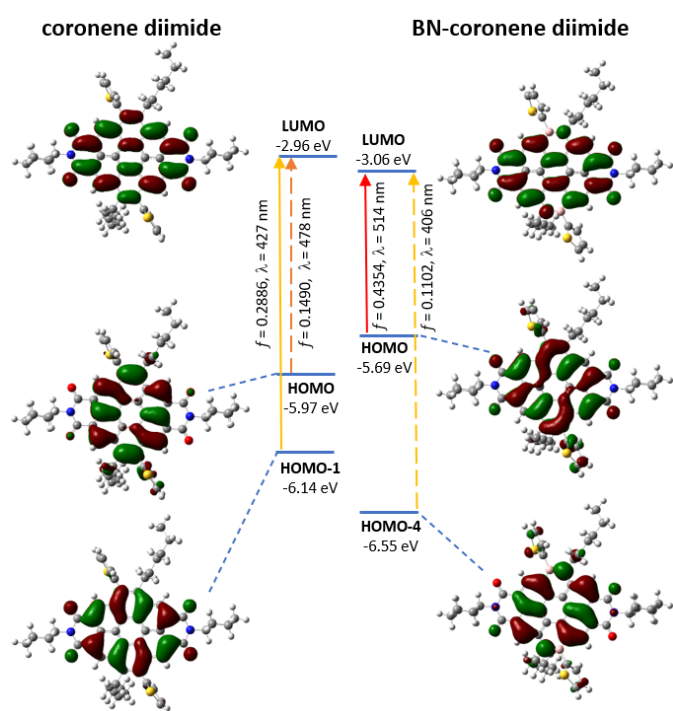
In general, the absorption maxima of the here presented **BNCDIs** were red-shifted compared to their CC-analog **CDI<sup>Dip</sup>** ( $\lambda_{\text{abs}} = 494 \text{ nm}$ ),<sup>62</sup> the **PDI<sup>Cy</sup>** ( $\lambda_{\text{abs}} = 525 \text{ nm}$ ),<sup>41</sup> the CN-isoster **diaza-CDI** ( $\lambda_{\text{abs}} = 488 \text{ nm}$ )<sup>63</sup> and previously reported BN-monosubstituted **BNPDI<sup>Cy</sup>** ( $\lambda_{\text{abs}} = 529 \text{ nm}$ )<sup>43</sup>. Compared to all carbon **PDI<sup>Dip</sup>** ( $\Phi_{\text{lum}} = 0.98$ )<sup>41</sup> and **CDI<sup>Dip</sup>** ( $\Phi_{\text{lum}} = 0.69$ )<sup>62</sup> similar or higher quantum yields were observed. However, the R-C=N-isosteric compound **CN-CDI** ( $\Phi_{\text{lum}} = 0.25$ )<sup>63</sup> was less emissive. Overall, the bathochromic shift of the absorption maxima  $\lambda_{\text{abs}}(\text{BNCDI}) = 535/538 \text{ nm}$  of the **BNCDIs** compared to the all-carbon **CDI** ( $\lambda_{\text{abs}}(\text{CDI}) = 494 \text{ nm}$ )<sup>62</sup> was distinct. This effect was attributed to the decrease of the HOMO-LUMO gap due to the BN units, an increased dipole moment but foremost to the orientation of the frontier orbitals (see below).

If one compares the characteristics of the absorption spectra of **BNCDIs** and **CDI**, systematic differences are found. In fact, the absorption spectra of both **BNCDIs** resembled more closely the absorption spectrum of a **PDI** than a **CDI**. Therefore, it was concluded that upon adding two BN units to a perylene core and extending the  $\pi$ -conjugated system in a lateral fashion, the absorption properties of the perylene core persist. This is not the case for the respective **CDI**. However, the absorption bands of **BNCDIs** at 350 nm and 425 nm are both absent in the absorption spectrum of **PDI** but are found in the absorption spectrum of the reported **CDI** unit.<sup>20, 62</sup> Therefore, it could be assumed that the absorption of a **PDI**-like ( $\lambda_{\text{abs}} \approx 530 \text{ nm}$ ) and the **CDI**-like systems ( $\lambda_{\text{abs}} \approx 425 \text{ nm}$ ) are both present in the

**Table 1** Overview of photophysical properties of both **BNCDIs**.

Compound	$\lambda_{\text{abs}}^a / \text{nm}$	$\text{Lg}(\epsilon)^a$	$E_{\text{opt}} / \text{eV}^b$	$\lambda_{\text{ems}}^a / \text{nm}$	$\Delta\nu_{\text{Stokes}}^a / \text{cm}^{-1}$	$\Phi_{\text{lum}}^c$
<b>BNCDI<sup>Cy</sup></b>	535	4.74	2.24	544	310	0.95
<b>BNCDI<sup>Dip</sup></b>	538	4.85	2.23	546	272	0.94

absorption of the **BNCDIs**. More details on this hypothesis will



be discussed below.

**Fig. 4** Display of the frontier orbitals of **BNCDI<sup>Cy</sup>** and **CDI<sup>Cy</sup>** calculated with B3LYP 6-31G\* at an isovalue of 0.02. The transitions calculated via TD-DFT are indicated.

### Theoretical Calculations

To understand the optoelectronic properties of **BNCDIs** in comparison with their C=C congener **CDI**, theoretical calculations using density functional theory (DFT) and time-dependent DFT (TD-DFT) were conducted. The ground state geometry was optimized, and the respective frontier orbitals and energies were extracted to investigate the effect of the BN units on the coronene core (Fig. 4). The electronic effect of the BN-substitution of the coronene core was clearly visible by comparing the LUMO/HOMO energy levels of **BNCDI** and **CDI**. It became evident that an isoelectronic substitution of two C=C-units by two BN units stabilized the LUMO level (-3.06 eV vs. -2.91 eV) and destabilized the HOMO level (-5.69 eV vs. -5.97 eV) resulting in a smaller HOMO-LUMO gap (2.63 eV vs. 3.06 eV).

To explain the absorption spectra of **CDI** and **BNCDI**, the frontier orbitals of both motifs were considered and TD-DFT calculations were performed. Initially, in both cases, the imide substituents displayed a node located at the imide's nitrogen which underlined the fact that imide substituents are barely interacting with the electrical features of these systems, which is in perfect agreement with the observed optical properties (Fig. 3).

The topology of the LUMO in both structures was similar to the one in rylene diimides<sup>20</sup> and therefore barely affected by the BN-substitution. In contrast, the nature of the HOMO changed drastically: The all-carbon coronene core of **CDI** exhibited a coronene-like organization of the HOMO whereas the HOMO

of the **BNCDI** was more related to the typical HOMO of **PDI**s<sup>64</sup>. In fact, the coronene-like topology in **CDIs** is the reason for a hypsochromic shifted absorption in contrast to common **PDI**s.<sup>20</sup> The respective coronene-like HOMO of the **BNCDI** was found in the HOMO-4 whereas the perylene-like HOMO of the **CDI** is displayed in the HOMO-1. Additionally, the present  $S_0 \rightarrow S_2$  transition (420 nm, Fig. 3), which might occur from the HOMO-4 to the LUMO level, and was similarly described for a more general **CDI** motif.<sup>21</sup> These findings were in agreement with the performed TD-DFT calculations which support the discrepancy between a coronene-like HOMO and a perylene-like LUMO indicated by the reduced oscillator strength (Fig. 4). Finally, this highlights how BN-units can shift the photophysical properties of PAHs by influencing the alignment of the frontier orbitals in addition to merely influencing the dipole moment. This could also explain the drastic bathochromic shifted absorption from **benzPDI** to its BN-congener **BNPDI**<sup>43</sup>. Furthermore, nuclear independent chemical shift (NICS)<sup>65-67</sup> calculations for both **BNCDI** and **CDI** were conducted. They revealed that the aromaticity of the annulated rings decreased for the BN-derivatives: The azaborine ring had a NICS(0) = -3.25 ppm and NICS(1) = -6.01 ppm whereas the same ring in the **CDI** showed a NICS(0) = -8.68 ppm and NICS(1) = -11.09 ppm. The reduced aromaticity of the BN-structure is a result of the more localized  $\pi$ -electrons on the B-N bond. A detailed NICS analysis of all rings for both **BNCDIs** and **CDIs** is shown in the ESI.

### Electrochemistry

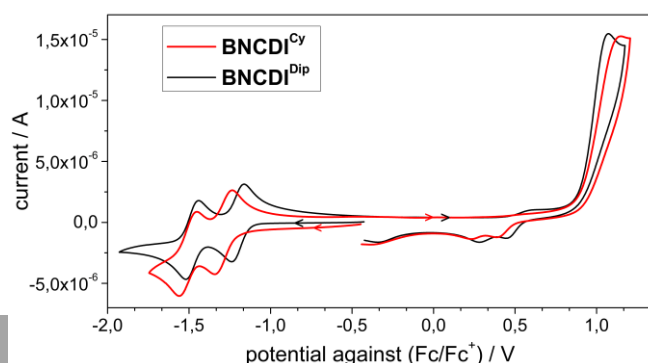
To further estimate the influence of the BN unit on the **CDI** motif, the redox properties of **BNCDI<sup>Cy</sup>** and **BNCDI<sup>Dip</sup>** were investigated using cyclic voltammetry experiments. Both **BNCDIs** exhibited two fully reversible distinctive reductive waves which is typical for rylene diimide systems<sup>54</sup> as both imides are reduced (Fig. 5). The onset potentials for the first reductive wave were  $E_{red, onset} = -1.10/-1.05$  V and therefore the energy level of the LUMO ( $E_{LUMO} = -3.69/-3.75$  eV) could be stimulated (Table 2). The electrochemical oxidation of both **BNCDIs** led to irreversible processes ( $E_{ox, onset} = 0.74/0.82$  V) giving rise to the respective HOMO levels ( $E_{HOMO} = -5.54/-5.62$  eV). Evidently, only a marginal effect of the imide substit-

**Table 2** Overview of electronic and thermal properties of both **BNCDIs**.

Compound	$E_{ox, onset}^a$ / eV	$E_{red, onset}^a$ / eV	$E_{LUMO}^b$ / eV	$E_{HOMO}^b$ / eV	$\Delta$ / eV	$T_{95}^c$ / °C
<b>BNCDI<sup>Cy</sup></b>	0.74	-1.10c	-3.69	-5.54	1.85	396
<b>BNCDI<sup>Dip</sup></b>	0.82	-1.05c	-3.75	-5.62	1.87	391

<sup>a</sup> In DCM with  $nBu_4NPF_6$  (0.2 M), a scan rate of 200 mV/s and ferrocene/ferrocenium as reference. For further details see ESI. <sup>b</sup> Derived from  $E_{LUMO} = -4.8$  eV -  $E_{red, onset}$  and  $E_{HOMO} = -4.8$  eV -  $E_{ox, onset}$ .<sup>68c</sup> See also footnote<sup>†</sup>. Temperature where 95% of the mass was still present at 10 K/min and 20 mL/min nitrogen flow.

**Fig. 5** Cyclic voltammogram of **BNCDI<sup>Cy</sup>** (red) and **BNCDI<sup>Dip</sup>** (black) in DCM with  $nBu_4NPF_6$  (0.2 M) as conducting salt using platinum working electrodes at 200mV/s sweep rate.



tments on the oxidation/reduction was found since the HOMO-LUMO gap was constant ( $\Delta E = 1.85/1.87$  eV). In comparison with the conventional **CDIs**, the LUMO level ( $E_{\text{LUMO}} = -3.69$  eV) was unchanged.<sup>42</sup> But since **CDIs** optical gap ( $E_{\text{opt}} = 2.46$  eV)<sup>42</sup> was larger than for the **BNCDis** ( $E_{\text{opt}} \approx 2.23$  eV), it can be concluded that the **BNCDis** have a destabilized HOMO and therefore lower the HOMO-LUMO gap. This was in good agreement with the calculation presented above.

The same trend was observed for the CN-isoster of the **BNCDis**, the **diaza-CDI**, where a similar LUMO level ( $E_{\text{LUMO}} = -3.69$  eV) and larger optical gap ( $E_{\text{opt}} = 2.47$  eV) were reported.<sup>63</sup> These electronic effects of the BN-substitution on the **CDI** were in great agreement with the above-mentioned theoretical investigations.

#### Optical Properties of the **BNCDis** in Aggregated State

Expecting increased luminescence response of the novel **BNCDis** at a lower temperature than at ambient conditions, we analyzed **BNCDis** using isopentane, which forms a glassy state when frozen, as solvent. Surprisingly, we observed complete luminescence quenching of the **BNCDis** at 150 K, where isopentane is still in a liquid state. Detailed temperature resolved investigation showed that the luminescence intensity decreases according to temperature but no appearance of other emission bands supporting an aggregation-caused quenching (ACQ)<sup>69, 70</sup> process due to the reduced solubility of the **BNCDis** was found. Further investigation showed that this quenching effect correlated with the nature of the imide group. The **BNCDI<sup>Cy</sup>** quenched its luminescence way faster than the **BNCDI<sup>Dip</sup>** upon cooling down (see ESI, Fig. S137). The result that emerges from these experiments was that the cyclohexyl substituent prevents less effectively the formation of aggregates than the diisopropylphenyl group and was an indication for the application in devices, where morphology effects are harder to predict. The initial observations on this ACQ behavior brought us to the idea to generate high luminescence solid-state materials by dispersing the **BNCDis** in poly(methylmethacrylate) (PMMA) matrix. The blending experiments were performed with dopant ratios of 0.75%, 1.5%, 4.8%, 9.0% and 50%). The emission properties of **BNCDI<sup>Cy</sup>** and **BNCDI<sup>Dip</sup>** in wavelength and intensities of the emitted light were visible to the naked eye (Fig. 6). In fact, the luminescence of the **BNCDI<sup>Dip</sup>** changed from yellow-greenish to a deep red while the luminescence of the **BNCDI<sup>Cy</sup>** was barely visible and underlined the aggregation-caused quenching in this **BNCDI** derivative. Compared to the optical properties observed in solution, a low amount of **BNCDI<sup>Cy</sup>** (0.75%) in PMMA resulted in

**Fig. 6** Image of the PMMA films with different weight ratios (from left to right: 0.75%, 1.5%, 4.8%, 9.0% and 50%) of both **BNCDis** under irradiation of UV light (365 nm) (top row: **BNCDI<sup>Cy</sup>**, bottom row: **BNCDI<sup>Dip</sup>**).

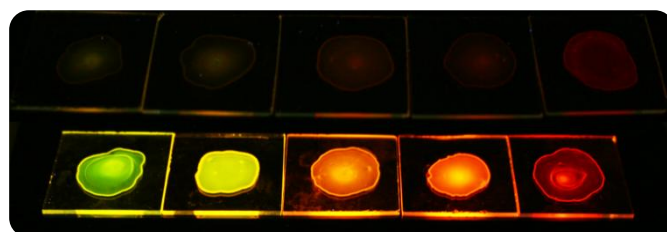
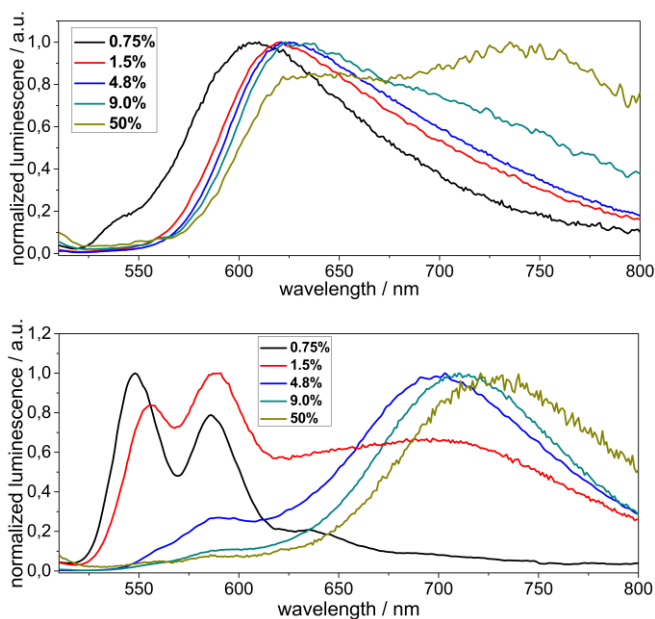


**Fig. 7** Emission spectra of the PMMA blends of **BNCDI<sup>Cy</sup>** (top) and **BNCDI<sup>Dip</sup>** (bottom) with different dopant ratios.

a red-shifted emission with a broad signal around 605 nm (Fig. 7, top). This represented a shift of approximately 80 nm towards the signal observed in DCM solution (Fig. 3) and might arise from aggregates emission.<sup>71</sup> Upon increasing the dopant rate, bathochromic shifts and broadening of the signals towards the NIR region were noticed. Using an equal amount of **BNCDI<sup>Cy</sup>** and PMMA a new band could be observed at 750 nm covering the whole emission spectra from 600 nm to 800 nm whilst the fluorescence was barely visible because of ACQ effects.

Repeating the experiment but changing the imide substituent from cyclohexyl to diisopropylphenyl moiety, drastic changes in the solid-state emission were observed. In the marginal dopant rate of 0.75%, the emission spectrum of **BNCDI<sup>Dip</sup>** was only slightly red-shifted (Fig. 7, bottom) and exhibited the same characteristics as in solution (Fig. 3). Since the vibronic transitions were clearly observable, it was assumed that only monomeric emission occurred. Doubling of the **BNCDI<sup>Dip</sup>** dopant rate (1.5%) resulted in a small bathochromic shift of the first emission band and an increase of the 0-1 transition. However, when such monomers begin to aggregate, the 0-1 transition commonly increases as it was for similar aggregated **PDIs**.<sup>72, 73</sup> Moreover, a new broad band arose (610-800 nm) with a maximum around 705 nm. With increasing the dopant rate an emission signal in the dark red region (690-730 nm) was visible which was, again, indicative for the aggregates emission.<sup>71</sup>

Comparing the experimental results for **BNCDI<sup>Cy</sup>** and **BNCDI<sup>Dip</sup>** several conclusions were drawn. For the same dopant ratios (0.75% and 1.5%) monomeric emission for **BNCDI<sup>Dip</sup>** was detected but not for **BNCDI<sup>Cy</sup>**. This led to the conclusion that the diisopropylphenyl substituent of **BNCDI<sup>Dip</sup>** was more efficient to prevent aggregation than the cyclohexyl-substituent of **BNCDI<sup>Cy</sup>**. This observation was in good agreement with knowledge obtained from the **PDI** derivatives.<sup>74</sup>

The difference between the **BNCDI<sup>Cy</sup>** and **BNCDI<sup>Dip</sup>** in the PMMA films was also investigated by optical microscopy. In the **BNCDI<sup>Cy</sup>/PMMA** blend needle-like agglomerates<sup>75</sup> were observed whereas nano-spheres<sup>76</sup> in the **BNCDI<sup>Dip</sup>/PMMA** blend could be detected (see ESI, Fig. SI36).

From the luminescence experiments at low temperature and in PMMA blends, the conclusion could be drawn that the imide substituents had a strong influence on the aggregation in the solid-state resulting in tuning the luminescence properties. These preliminary experiments were good indicators for the performance of both **BNCDIs** in organic light-emitting diodes (OLEDs).

#### Thermal properties

The thermal properties of both **BNCDIs** were investigated to evaluate their stability towards evaporation for organic devices. For both **BNCDIs** decomposition occurred at temperatures higher than 390 °C, indicated by 5% mass loss which are comparable to the respective **PDI<sup>Dip</sup>** and **PDI<sup>Cy</sup>** (see ESI, Fig. SI44). This analysis underlines the concept of condensing labile azaborine units with thermally stable PAH structures and suggested sufficient stability for thermal evaporation processes. Additionally, in a dynamic scanning calorimetry (DSC) experiment, no glass-transition temperature ( $T_g$ ) in the range of -80 °C to 300 °C could be measured (see ESI, Fig. SI45 and SI46). Due to their amorphous characteristics, their morphological stability during the fabrication processing of OLEDs was therefore envisaged.

#### Organic Field Effect Transistor (OFET)

To study the charge transport ability of **BNCDIs**, the material that was shown to aggregate more, **BNCDI<sup>Cy</sup>** was integrated into a bottom-gate bottom-contact n-type OFET device. The characteristics of the OFET were measured in linear and saturated regime (i.e.  $V_{DS} = 20$  V and  $V_{DS} = 50$  V).

The linear field-effect mobility was estimated to be  $\mu_{FE} = 1.02 \times 10^{-8} \text{ cm}^2 \text{ V}^{-1} \text{ s}^{-1}$  while in the saturated regime, field-effect mobility was  $\mu_{FE} = 4.34 \times 10^{-8} \text{ cm}^2 \text{ V}^{-1} \text{ s}^{-1}$ . The classical electrical parameters of OFET were defined by its low conductivity ( $\mu_e = 3.42 \times 10^{-6} \text{ cm}^2 \text{ V}^{-1} \text{ s}^{-1}$ ), low on/off-current ratio ( $I_{on}/I_{off} = 36$ ) and high threshold voltage ( $V_{th} \approx 21$  V). The OFET device was also annealed at 150 °C to induce

reorganization of the semiconducting layer. At this temperature, the linear field-effect mobility was slightly increased to  $\mu_{FE} = 2.68 \times 10^{-8} \text{ cm}^2 \text{ V}^{-1} \text{ s}^{-1}$  and the threshold voltage was shifted ( $V_{th} \approx 16$  V) due to a decreased defect density in the device. This result showed that the **BNCDIs** in general are capable of electron transportation in organic devices.

#### Organic Light Emitting Diode (OLED)

After the preliminary evaluation of the solid-state luminescence in the PMMA matrix had revealed promising optoelectronic and thermal properties, we used both **BNCDIs** in multilayer organic light-emitting devices (OLEDs). Because no oxidation was recorded, the use of a host matrix with matching HOMO-LUMO levels was necessary; moreover; this was expected to prevent ACQ effects. Therefore, 4,4'-bis(*N*-carbazolyl)-1,1'-biphenyl (**CBP**) or 4,4'-bis(2,2-diphenylvinyl)-1,1'-biphenyl (**DPVBi**) were used as host and the respective **BNCDIs** as guest.

The general set-up for the OLEDs was ITO/CuPc (10 nm)/ $\alpha$ -NPB (40 nm)/ TCTA (10 nm)/EML (20 nm)/ TPBi (50 nm)/LiF (1.2 nm)/Al (100 nm) (see ESI). We co-sublimed the **BNCDIs** with two different blue-matrices defining the weight-ratio by adjusting the partial pressure of the respective substrates.

The first OLED devices (**A-B**) with doping ratios of 1.5% and 3% **BNCDI<sup>Cy</sup>** were constructed with **CBP** as a matrix to a draw direct conclusion to the reported **BNPDI<sup>Cy</sup>** OLED<sup>43</sup>. The observed electroluminescence spectra revealed two main emission bands at 400 nm, arising from the host, and a broader emission at 550 nm from the **BNCDI<sup>Cy</sup>** (Fig. 8, left). The occurrence of the host's emission indicated insufficient charge transfer or aggregation in the device. However, the increase of the doping ratio (device A/B) decreased the performance of the OLED. The luminance (442/317 cd/m<sup>2</sup>) and the EQE (0.7/0.6%) of both devices were at a low level compared to the reported **BNPDI<sup>Cy</sup>** OLED (EQE values up to 1.5% and luminance (>1000 cd/m<sup>2</sup>)).<sup>43</sup>

Since these devices' performances were insufficient, another host (**DPVBi**) was used as a matrix and with a dopant rate from 1.1% to 9.3% **BNCDI<sup>Cy</sup>** (devices **C-E**, Fig. 8, middle). The observed electroluminescence for device **C** showed two significant bands at 450 nm, from the host, and 540 nm, from **BNCDI<sup>Cy</sup>**, resulting in a turquoise light ( $x = 0.252$ ,  $y = 0.344$ ). Device **C** exhibited an EQE of 1.4%, a brightness of 1001 cd m<sup>-2</sup>, low turn-on voltage ( $V_{on} = 4.2$  V) and a power efficiency of 1.3 lm W<sup>-1</sup>. The raise of the dopant rate to 9.3% (device **E**) decreased the overall performance of the device (Table 3). Presumably, with a higher dopant ratio of **BNCDI<sup>Cy</sup>**, ACQ processes are favoured which was

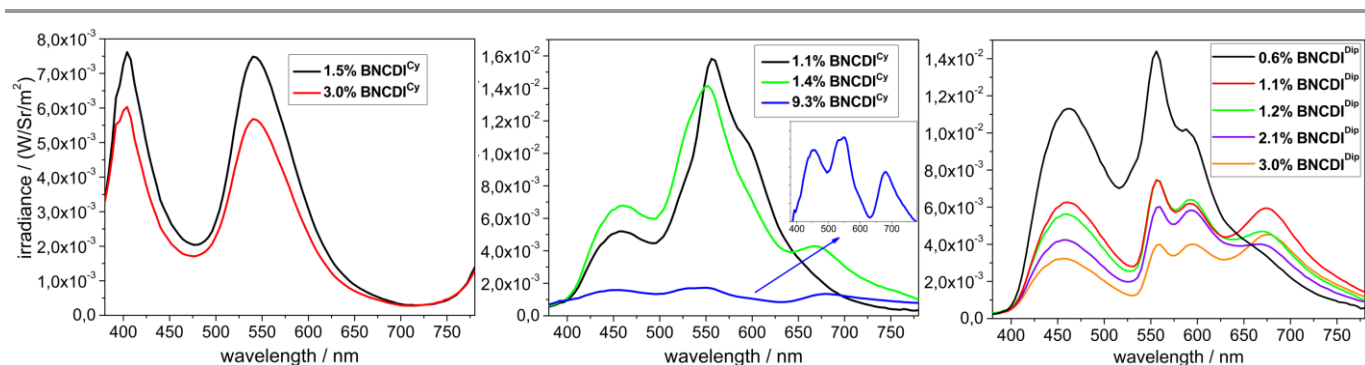


**Fig. 8** Electroluminescence spectra of devices **A-B** (left) with **BNCIDI<sup>Cy</sup>** and **CBP** matrix, devices **C-E** (middle) with **BNCIDI<sup>Cy</sup>** and **DPVBi** matrix, devices **G-J** (right) with different dopant rate of **BNCIDI<sup>Dip</sup>** in **DPVBi** matrix.

**Table 3** Electroluminescent performance of devices **A-J**. The best parameters are highlighted bold.

Host	Doping ratio (%)	EQE <sup>a</sup> (%)	cd/A <sup>a</sup>	lm/W <sup>a</sup>	V <sub>on</sub> <sup>b</sup> (V)	Luminance <sup>c</sup> (cd/m <sup>2</sup> )	CIE <sup>c</sup> (x; y)
<b>CBP:</b> <b>BNCIDI<sup>Cy</sup></b>	1.5 <b>A</b>	0.7	1.5	0.5	5.0	442	0.309; 0.415
	3.0 <b>B</b>	0.6	1.3	0.4	6.0	371	0.308; 0.417
<b>DPVBi:</b> <b>BNCIDI<sup>Cy</sup></b>	1.1 <b>C</b>	1.4	<b>3.3</b>	<b>1.3</b>	4.2	<b>1001</b>	0.374; 0.431
	1.4 <b>D</b>	1.4	2.7	1.1	4.3	842	0.327; 0.416
	9.3 <b>E</b>	0.3	0.4	0.1	4.8	117	0.298; 0.339
<b>DPVBi:</b> <b>BNCIDI<sup>Dip</sup></b>	0.6 <b>F</b>	<b>1.5</b>	2.7	<b>1.3</b>	3.7	800	<b>0.317; 0.346</b>
	1.1 <b>G</b>	1.3	1.8	0.9	3.7	530	0.347; 0.336
	1.2 <b>H</b>	1.1	1.6	0.7	<b>3.6</b>	480	0.357; 0.336
	2.1 <b>I</b>	0.9	1.3	0.6	3.7	380	0.376; 0.342
	3.0 <b>J</b>	0.8	1.0	1.0	0.5	4.0	275

<sup>a</sup> Recorded at 10 mA/cm<sup>2</sup>. <sup>b</sup> Recorded at luminance of 0.1 cd/m<sup>2</sup> (± 0.2 V). <sup>c</sup> Recorded at 30 mA/cm<sup>2</sup>.

expected from the experiments in the PMMA blend and as well in the OLED consisting of **BNPDI<sup>Cy</sup>**.<sup>43</sup> Since the best matrix/dopant interaction was obtained with **DPVBi** in the previous devices, devices **F-J** with **BNCIDI<sup>Dip</sup>** were fabricated with the same matrix. Since the only difference between **BNCIDI<sup>Cy</sup>** and **BNCIDI<sup>Dip</sup>** was in their supramolecular arrangement and not their optoelectronic properties, a direct conclusion towards the effect of the imide bands can be drawn. Interestingly, device **F** exhibited also two main bands located at 460 nm and with slightly higher intensity at 560 nm resulting from the matrix and the **BNCIDI<sup>Dip</sup>** (Fig. 8, right). The latter band showed a small shoulder which might be related to the vibronic structure of the **BNCIDI** core. The CIE coordinates (device **F**: x = 0.317; y = 0.346) are close to white light (x = 0.330; y = 0.330). Moreover, device **F** exhibited an EQE of 1.5%, a brightness of 800 cd m<sup>-2</sup>, and a power efficiency of 1.3 lm W<sup>-1</sup>. Upon increasing the amount of **BNCIDI<sup>Dip</sup>** (devices **G-J**) the overall intensity decreased whereas a new band at 690 nm occurred. This might be related to aggregation processes since a similar band was observed in the blend of **BNCIDI<sup>Dip</sup>** with PMMA (Fig. 7). By increasing the dopant ratio, the performance of these devices decreased significantly. Interestingly, devices **G-J** showed light emission at the region

of white light (all CIE charts are to be in the ESI, Fig. S152 and S153).

#### Discussion of the device performances

The observed smaller HOMO-LUMO gap induced by the lateral BN-expansion of a **PDI** to a **BNCIDI** and enhanced photophysical properties compared to the **CDI** motif could be transferred to several organic light-emitting devices using a host-guest set-up. We observed, however, that the integration of two hexyl chains on the BN-motif could not overcome the general problem of aggregation which is common in rylene diimides due to strong  $\pi$ - $\pi$  interactions. This diminished the performance of the OLED devices with increasing doping rate of **BNCIDI**. This is in line with the poor electron mobility ( $\mu_e = 10^{-6}$  cm<sup>2</sup> V<sup>-1</sup> s<sup>-1</sup>) of the neat material in an OFET device which is most likely due to morphological disadvantages. Furthermore, this is also supported by the fact that an improved performance after the reorganization of the film via annealing was observed (see ESI). To obtain higher electron mobility, appropriate (fluorinated) alkyl chains could be introduced to the nitrogen atom of the BN-motif or on the imide position of the **BNCIDI**. While this is likely to increase OFET performance, a decrease in the performance in an OLED device due to a dense packing of the cores is to be expected.

Despite advantages in fluorescence quantum yields and excitation energy gap reduction, a planar BN-coronene core in itself seems insufficient to increase the electron mobility; the values obtained by us are similar to a structurally similar thiophene-substituted **PDI** ( $\mu_e = 10^{-6} \text{ cm}^2 \text{ V}^{-1} \text{ s}^{-1}$ ) to **CDI** ( $\mu_e = 10^{-4} \text{ cm}^2 \text{ V}^{-1} \text{ s}^{-1}$ ).<sup>77</sup>

However, in combination with matrices, better OLED performance properties could be accessed (EQE up to 1.5%) compared to common **PDI**s (EQE up to 0.638%)<sup>78</sup> or heteroatom bay-annulated **PDI** (EQE up to 0.06%).<sup>79</sup>

## Conclusions

In summary, we present the synthesis of regioisomerically pure **BNCDI**s via a BN-annulation reaction starting from **PDI** precursors. Initially, the optoelectronic properties **BNCDI**s were investigated and compared to its all-carbon coronene diimides: A large bathochromic shift (40 nm) and a higher  $\epsilon$  compared to their carbonaceous congeners were observed. In fact, it was found that the BN-extension overcame the inferior photophysical properties which were observed for the CC-extension from **PDI** to **CDI**. DFT calculations showed that the BN-substitution stabilized a perylene-like HOMO whereas a CC-substitution leads to a coronene-like HOMO. This concept might be extendable to all cases where lateral  $\pi$ -extension of PAHs leads to inferior optical properties.

Moreover, the effect of the imide substituents (cyclohexyl or diisopropylphenyl) for the **BNCDI**s was investigated in solution (ambient and low temperature) and solid-state matrices (OLEDs and PMMA): It was found that the cyclohexyl motif was less effective in preventing aggregation-caused quenching (ACQ) than the diisopropylphenyl substituent.

In addition to the examination of their redox properties, thermal stability ( $T_{95} > 390 \text{ }^\circ\text{C}$ ), the charge transfer behaviour was investigated in a n-type OFET ( $\mu_e = 10^{-6} \text{ cm}^2 \text{ V}^{-1} \text{ s}^{-1}$ ). The rich chemistry for postfunctionalization of rylene diimides<sup>80</sup> should allow further modification for this n-type organic semiconductor to access lower lying LUMOs by stabilizing it with cyano groups<sup>81</sup> or halides.<sup>82</sup>

Both **BNCDI**s were deployed in host matrices in a multi-stack OLED setup. Apart from being non-luminescent in the aggregated state, by blending the **BNCDI**s with a blue-emitting matrix it was demonstrated that white light emission in a multi-layered OLED device ( $x = 0.317$ ;  $y = 0.346$ ) could be achieved. Overall, the OLED performance was characterized with a maximum EQE of 1.5%, low turn-on voltage ( $V_{\text{on}} = 3.6 \text{ V}$ ) and a luminance up to  $1001 \text{ cd/m}^2$ . However, to further increase the efficiency of **BNCDI**s in OFETs/OLEDs, modification of the imide function, e.g. by sterically demanding terphenyl imide substituents,<sup>52, 83</sup> can be directly implemented.

## Conflicts of Interest

There are no conflicts to declare.

## Acknowledgements

The Authors thank Prof. F. Sönnichsen and his support with the <sup>11</sup>B NMR measurements. A. S. thanks the German research Foundation (DFG) for and Emmy-Noether grant (STA1195/2-1). J.H. acknowledges funding for a Short-Term Scientific Mission from the COST action COST 1302: "European Network on Smart Inorganic Polymers". This work is supported by the Ministère de la Recherche et de l'Enseignement Supérieur, the CNRS, the Region Bretagne, and COST CM 1302 (SIPS).

## Notes and References

1. C. Aumaitre, J. F. Morin, *Chem. Rec.*, **2019**, *19*, 1142-1154.
2. J. Mei, Y. Diao, A. L. Appleton, L. Fang, Z. Bao, *J. Am. Chem. Soc.*, **2013**, *135*, 6724-6746.
3. M. Stepien, E. Gonka, M. Zyla, N. Sprutta, *Chem. Rev.*, **2017**, *117*, 3479-3716.
4. C. Wang, H. Dong, W. Hu, Y. Liu, D. Zhu, *Chem. Rev.*, **2012**, *112*, 2208-2267.
5. J. E. Anthony, *Chem. Rev.*, **2006**, *106*, 5028-5048.
6. J. Roncali, *Chem. Rev.*, **1997**, *97*, 173-206.
7. J. Wu, W. Pisula, K. Müllen, *Chem. Rev.*, **2007**, *107*, 718-747.
8. A. Narita, X. Y. Wang, X. Feng, K. Müllen, *Chem. Soc. Rev.*, **2015**, *44*, 6616-6643.
9. L. Schmidt-Mende, A. Fechtenkötter, K. Müllen, E. Moons, R. H. Friend, J. D. MacKenzie, *Science*, **2001**, *293*, 1119-1122.
10. K. Müllen, U. Scherf, *Organic Light Emitting Devices: Synthesis, Properties and Applications*, Wiley VCH, Weinheim, **2005**.
11. M. Chen, L. Yan, Y. Zhao, I. Murtaza, H. Meng, W. Huang, *J. Mater. Chem. C*, **2018**, *6*, 7416-7444.
12. A. Herrmann, K. Müllen, *Chem. Lett.*, **2006**, *35*, 978-985.
13. C. Jung, B. K. Muller, D. C. Lamb, F. Nolde, K. Müllen, C. Brauchle, *J. Am. Chem. Soc.*, **2006**, *128*, 5283-5291.
14. T. Weil, T. Vosch, J. Hofkens, K. Peneva, K. Müllen, *Angew. Chem. Int. Ed.*, **2010**, *49*, 9068-9093.
15. X. Zhan, A. Facchetti, S. Barlow, T. J. Marks, M. A. Ratner, M. R. Wasielewski, S. R. Marder, *Adv. Mater.*, **2011**, *23*, 268-284.
16. A. Nowak-Krol, K. Shoyama, M. Stolte, F. Würthner, *Chem. Commun.*, **2018**, *54*, 13763-13772.
17. S. Müller, K. Müllen, *Chem. Commun.*, **2005**, 4045-4046.
18. L. Chen, C. Li, K. Müllen, *J. Mater. Chem. C*, **2014**, *2*, 1938-1956.
19. H. Langhals, S. Kirner, *Eur. J. Org. Chem.*, **2000**, *2000*, 365-380.
20. M. Adachi, Y. Nagao, *Chem. Mater.*, **2001**, *13*, 662-669.
21. J. Calbo, A. Doncel-Giménez, J. Aragó, E. Ortí, *Theor. Chem. Acc.*, **2018**, *137*.
22. M. Hirai, N. Tanaka, M. Sakai, S. Yamaguchi, *Chem. Rev.*, **2019**, *119*, 8291-8331.
23. Z. Liu, T. B. Marder, *Angew. Chem. Int. Ed.*, **2008**, *47*, 242-244.
24. P. G. Campbell, A. J. Marwitz, S. Y. Liu, *Angew Chem Int Ed Engl*, **2012**, *51*, 6074-6092.
25. M. M. Morgan, W. E. Piers, *Dalton Trans.*, **2016**, *45*, 5920-5924.
26. M. J. D. Bosdet, W. E. Piers, *Can. J. Chem.*, **2009**, *87*, 8-29.

27. P. F. Zhang, F. D. Zhuang, Z. H. Sun, Y. Lu, J. Y. Wang, J. Pei, *J. Org. Chem.*, **2020**, *85*, 241-247.
28. J. S. Ishibashi, J. L. Marshall, A. Maziere, G. J. Lovinger, B. Li, L. N. Zakharov, A. Dargelos, A. Graciaa, A. Chrostowska, S. Y. Liu, *J. Am. Chem. Soc.*, **2014**, *136*, 15414-15421.
29. X.-Y. Wang, F.-D. Zhuang, X. Zhou, D.-C. Yang, J.-Y. Wang, J. Pei, *J. Mater. Chem. C*, **2014**, *2*, 8152-8161.
30. F. D. Zhuang, Z. H. Sun, Z. F. Yao, Q. R. Chen, Z. Huang, J. H. Yang, J. Y. Wang, J. Pei, *Angew. Chem. Int. Ed.*, **2019**, *58*, 10708-10712.
31. A. Abengozar, P. Garcia-Garcia, D. Sucunza, L. M. Frutos, O. Castano, D. Sampedro, A. Perez-Redondo, J. J. Vaquero, *Org. Lett.*, **2017**, *19*, 3458-3461.
32. F. D. Zhuang, J. H. Yang, Z. H. Sun, P. F. Zhang, Q. R. Chen, J. Y. Wang, J. Pei, *Chin. J. Chem.* **2021**, *39*, 909-912.
33. M. Baranac-Stojanovic, *Chemistry*, **2014**, *20*, 16558-16565.
34. M. Stojanović, M. Baranac-Stojanović, *New J. Chem.*, **2018**, *42*, 12968-12976.
35. C. J. Saint-Louis, L. L. Magill, J. A. Wilson, A. R. Schroeder, S. E. Harrell, N. S. Jackson, J. A. Trindell, S. Kim, A. R. Fisch, L. Munro, V. J. Catalano, C. E. Webster, P. P. Vaughan, K. S. Molek, A. K. Schrock, M. T. Huggins, *J. Org. Chem.*, **2016**, *81*, 10955-10963.
36. X. Y. Wang, H. R. Lin, T. Lei, D. C. Yang, F. D. Zhuang, J. Y. Wang, S. C. Yuan, J. Pei, *Angew. Chem. Int. Ed.*, **2013**, *52*, 3117-3120.
37. X. Y. Wang, F. D. Zhuang, R. B. Wang, X. C. Wang, X. Y. Cao, J. Y. Wang, J. Pei, *J. Am. Chem. Soc.*, **2014**, *136*, 3764-3767.
38. A. Abengozar, P. Garcia-Garcia, D. Sucunza, A. Perez-Redondo, J. J. Vaquero, *Chem. Commun.*, **2018**, *54*, 2467-2470.
39. Y. Appiaris, T. Stauch, E. Lork, P. Rusch, N. C. Bigall, A. Staubitz, *Org. Chem. Front.*, **2021**, *8*, 10-17.
40. M. J. Bosdet, C. A. Jaska, W. E. Piers, T. S. Sorensen, M. Parvez, *Org. Lett.*, **2007**, *9*, 1395-1398.
41. A. Rademacher, S. Märkle, H. Langhals, *Chem. Ber.*, **1982**, *115*, 2927-2934.
42. Y. Avlasevich, C. Li, K. Müllen, *J. Mater. Chem.*, **2010**, *20*, 3814.
43. G. Li, Y. Zhao, J. Li, J. Cao, J. Zhu, X. W. Sun, Q. Zhang, *J. Org. Chem.*, **2015**, *80*, 196-203.
44. Y. Huang, J. Xing, Q. Gong, L. C. Chen, G. Liu, C. Yao, Z. Wang, H. L. Zhang, Z. Chen, Q. Zhang, *Nat. Commun.*, **2019**, *10*, 169.
45. Q. Zhao, S. Zhang, Y. Liu, J. Mei, S. Chen, P. Lu, A. Qin, Y. Ma, J. Z. Sun, B. Z. Tang, *J. Mater. Chem.*, **2012**, *22*, 7387.
46. J. Ide, R. Mereau, L. Ducasse, F. Castet, Y. Olivier, N. Martinelli, J. Cornil, D. Beljonne, *J. Phys. Chem. B*, **2011**, *115*, 5593-5603.
47. Z. Chen, V. Stepanenko, V. Dehm, P. Prins, L. D. Siebbeles, J. Seibt, P. Marquetand, V. Engel, F. Würthner, *Chemistry*, **2007**, *13*, 436-449.
48. F. Zhang, Y. Ma, Y. Chi, H. Yu, Y. Li, T. Jiang, X. Wei, J. Shi, *Sci. Rep.*, **2018**, *8*, 8208.
49. M. J. Lin, A. Jimenez, C. Burschka, F. Würthner, *Chem. Commun.*, **2012**, *48*, 12050-12052.
50. S. Nakazono, S. Easwaramoorthi, D. Kim, H. Shinokubo, A. Osuka, *Org. Lett.*, **2009**, *11*, 5426-5429.
51. X. Li, H. Wang, J. A. Schneider, Z. Wei, W.-Y. Lai, W. Huang, F. Wudl, Y. Zheng, *J. Mater. Chem. C*, **2017**, *5*, 2781-2785.
52. B. Zhang, H. Soleimaninejad, D. J. Jones, J. M. White, K. P. Ghiggino, T. A. Smith, W. W. H. Wong, *Chem. Mater.*, **2017**, *29*, 8395-8403.
53. J. L. Banal, H. Soleimaninejad, F. M. Jradi, M. Liu, J. M. White, A. W. Blakers, M. W. Cooper, D. J. Jones, K. P. Ghiggino, S. R. Marder, T. A. Smith, W. W. H. Wong, *J. Phys. Chem. C*, **2016**, *120*, 12952-12958.
54. S. K. Lee, Y. Zu, A. Herrmann, Y. Geerts, K. Müllen, A. J. Bard, *J. Am. Chem. Soc.*, **1999**, *121*, 3513-3520.
55. S. Sengupta, R. K. Dubey, R. W. Hoek, S. P. van Eeden, D. D. Gunbas, F. C. Grozema, E. J. Sudholter, W. F. Jager, *J. Org. Chem.*, **2014**, *79*, 6655-6662.
56. M. J. Ahrens, M. J. Tauber, M. R. Wasielewski, *J. Org. Chem.*, **2006**, *71*, 2107-2114.
57. P. Xiao, F. Dumur, B. Graff, D. Gigmès, J. P. Fouassier, J. Lalevee, *Macromol. Rapid Commun.*, **2013**, *34*, 1452-1458.
58. H. Wang, T. E. Kaiser, S. Uemura, F. Würthner, *Chem. Commun.*, **2008**, 1181-1183.
59. J. Seibt, P. Marquetand, V. Engel, Z. Chen, V. Dehm, F. Würthner, *Chem. Phys.*, **2006**, *328*, 354-362.
60. H. Langhals, *Heterocycles*, **1995**, *40*, 477.
61. R. Gvishi, R. Reisfeld, Z. Burshtein, *Chem. Phys. Lett.*, **1993**, *213*, 338-344.
62. C. L. Eversloh, C. Li, K. Müllen, *Org. Lett.*, **2011**, *13*, 4148-4150.
63. L. Hao, W. Jiang, Z. Wang, *Tetrahedron*, **2012**, *68*, 9234-9239.
64. F. Würthner, C. R. Saha-Moller, B. Fimmel, S. Ogi, P. Leowanawat, D. Schmidt, *Chem. Rev.*, **2016**, *116*, 962-1052.
65. P. V. R. Schleyer, C. Maerker, A. Dransfeld, H. Jiao, N. J. R. van Eikema Hommes, *J. Am. Chem. Soc.*, **1996**, *118*, 6317-6318.
66. B. Goldfuss, P. v. R. Schleyer, *Organometallics*, **1997**, *16*, 1543-1552.
67. P. V. R. Schleyer, M. Manoharan, Z. X. Wang, B. Kiran, H. Jiao, R. Puchta, N. J. R. van Eikema Hommes, *Org. Lett.*, **2001**, *3*, 2465-2468.
68. J. L. Bredas, R. Silbey, D. S. Boudreaux, R. R. Chance, *J. Am. Chem. Soc.*, **1983**, *105*, 6555-6559.
69. Y. Hong, J. W. Lam, B. Z. Tang, *Chem. Soc. Rev.*, **2011**, *40*, 5361-5388.
70. Y. Hong, J. W. Lam, B. Z. Tang, *Chem. Commun.*, **2009**, 4332-4353.
71. J. Sung, P. Kim, B. Fimmel, F. Würthner, D. Kim, *Nat. Commun.*, **2015**, *6*, 8646.
72. Y.-S. Ma, C.-H. Wang, Y.-J. Zhao, Y. Yu, C.-X. Han, X.-J. Qiu, Z. Shi, *Supramol. Chem.*, **2007**, *19*, 141-149.
73. F. Würthner, C. R. Saha-Möller, B. Fimmel, S. Ogi, P. Leowanawat, D. Schmidt, *Chem. Rev.*, **2015**, *116*, 962-1052.
74. Z. Chen, B. Fimmel, F. Würthner, *Org. Biomol. Chem.*, **2012**, *10*, 5845-5855.
75. A. L. Briseno, S. C. Mannsfeld, C. Reese, J. M. Hancock, Y. Xiong, S. A. Jenekhe, Z. Bao, Y. Xia, *Nano Lett.*, **2007**, *7*, 2847-2853.
76. Y. Yu, Y. Li, Z. Qin, R. Jiang, H. Liu, Y. Li, *J. Colloid Interface Sci.*, **2013**, *399*, 13-18.

77. T. Ogawa, D. Kuzuhara, *ChemPlusChem*, **2021**, *86*, 852-857.
78. E. Kozma, W. Mróz, F. Villafiorita-Monteleone, F. Galeotti, A. Andicsová-Eckstein, M. Catellani, C. Botta, *RSC Adv.*, **2016**, *6*, 61175-61179.
79. S. V. Dayneko, M. Rahmati, M. Pahlevani, G. C. Welch, *J. Mater. Chem. C*, **2020**, *8*, 2314-2319.
80. A. Nowak-Król, F. Würthner, *Org. Chem. Front.*, **2019**, *6*, 1272-1318.
81. J. Gao, C. Xiao, W. Jiang, Z. Wang, *Org. Lett.*, **2014**, *16*, 394-397.
82. R. Schmidt, J. H. Oh, Y. S. Sun, M. Deppisch, A. M. Krause, K. Radacki, H. Braunschweig, M. Konemann, P. Erk, Z. Bao, F. Würthner, *J. Am. Chem. Soc.*, **2009**, *131*, 6215-6228.
83. Y. Zheng, F. M. Jradi, T. C. Parker, S. Barlow, S. R. Marder, S. S. Saavedra, *ACS Appl. Mater. Interfaces*, **2016**, *8*, 34089-34097.

## Footnote

<sup>†</sup> Electronic supplementary information (ESI) available. See DOI: 10.1039/x0xx00000x

<sup>‡</sup> Although this is often referred to as the LUMO, and Table 2 is resented as  $E_{\text{LUMO}}$ , we wish to point out that actually the LUMO cannot be measured in this way, as it is not defined electrochemically.